Nonlinear responses in optical metamaterials: theory and experiment

Shiwei Tang,[1] David J. Cho,[2] Hao Xu,[1] Wei Wu,[3] Y. Ron Shen,[2] and Lei Zhou[1,*]

[1]*State Key Laboratory of Surface Physics and Key Laboratory of Micro and Nano Photonic Structures (Ministry of Education), Fudan University, Shanghai 200433, China*
[2]*Department of Physics, University of California, Berkeley, California 94720, USA*
[3]*Quantum Science Research, Hewlett-Packard Laboratories, Palo Alto, California 94304, USA*
**phzhou@fudan.edu.cn*

Abstract: We employed both theoretical calculations and experiments to study the nonlinear responses in optical metamaterials. The spectra of second-harmonic generations measured on a fishnet metamaterial are in *quantitative* agreements with calculations based on full-wave numerical simulations combined with field integrations, both exhibiting ~80 times enhancements at the magnetic resonance frequency. Our calculations explained several interesting features observed experimentally, and suggested an optimal metamaterial structure to yield the strongest nonlinear signals.

OCIS codes: (160.3918) Metamaterials; (190.0190) Nonlinear optics; (260.5740) Resonance.

References and links

1. D. R. Smith, W. J. Padilla, D. C. Vier, S. C. Nemat-Nasser, and S. Schultz, "Composite medium with simultaneously negative permeability and permittivity," Phys. Rev. Lett. **84**(18), 4184–4187 (2000).
2. R. A. Shelby, D. R. Smith, and S. Schultz, "Experimental verification of a negative index of refraction," Science **292**(5514), 77–79 (2001).
3. J. B. Pendry, "Negative refraction makes a perfect lens," Phys. Rev. Lett. **85**(18), 3966–3969 (2000).
4. T. J. Yen, W. J. Padilla, N. Fang, D. C. Vier, D. R. Smith, J. B. Pendry, D. N. Basov, and X. Zhang, "Terahertz magnetic response from artificial materials," Science **303**(5663), 1494–1496 (2004).
5. S. Linden, C. Enkrich, M. Wegener, J. Zhou, T. Koschny, and C. M. Soukoulis, "Magnetic response of metamaterials at 100 terahertz," Science **306**(5700), 1351–1353 (2004).
6. C. Enkrich, M. Wegener, S. Linden, S. Burger, L. Zschiedrich, F. Schmidt, J. F. Zhou, Th. Koschny, and C. M. Soukoulis, "Magnetic metamaterials at telecommunication and visible frequencies," Phys. Rev. Lett. **95**(20), 203901 (2005).
7. A. N. Grigorenko, A. K. Geim, H. F. Gleeson, Y. Zhang, A. A. Firsov, I. Y. Khrushchev, and J. Petrovic, "Nanofabricated media with negative permeability at visible frequencies," Nature **438**(7066), 335–338 (2005).
8. M. W. Klein, C. Enkrich, M. Wegener, C. M. Soukoulis, and S. Linden, "Single-slit split-ring resonators at optical frequencies: limits of size scaling," Opt. Lett. **31**(9), 1259–1261 (2006).
9. W. J. Padilla, A. J. Taylor, C. Highstrete, M. Lee, and R. D. Averitt, "Dynamical electric and magnetic metamaterial response at terahertz frequencies," Phys. Rev. Lett. **96**(10), 107401 (2006).
10. D. R. Smith, S. Schultz, P. Markos, and C. M. Soukoulis, "Determination of effective permittivity and permeability of metamaterials from re⟩ection and transmission coef□cients," Phys. Rev. B **65**(19), 195104 (2002).
11. S. O'Brien, D. McPeake, S. A. Ramakrishna, and J. B. Pendry, "Near-infrared photonic band gaps and nonlinear effects in negative magnetic metamaterials," Phys. Rev. B **69**(24), 241101 (2004).
12. J. Zhou, Th. Koschny, M. Kafesaki, E. N. Economou, J. B. Pendry, and C. M. Soukoulis, "Saturation of the magnetic response of split-ring resonators at optical frequencies," Phys. Rev. Lett. **95**(22), 223902 (2005).
13. J. B. Pendry, D. Schurig, and D. R. Smith, "Controlling electromagnetic fields," Science **312**(5781), 1780–1782 (2006).
14. D. Schurig, J. J. Mock, B. J. Justice, S. A. Cummer, J. B. Pendry, A. F. Starr, and D. R. Smith, "Metamaterial electromagnetic cloak at microwave frequencies," Science **314**(5801), 977–980 (2006).
15. H. Q. Lei Zhou, "Li, Y. Q. Qin, Z. Y. Wei, and C. T. Chan, "Directive emissions from subwavelength metamaterial-based cavities," Appl. Phys. Lett. **86**, 101101 (2005).
16. J. B. Pendry, A. J. Holden, D. J. Robbins, and W. J. Stewart, "Magnetism from conductors and enhanced nonlinear phenomena," IEEE Trans. Microw. Theory Tech. **47**(11), 2075–2084 (1999).
17. M. W. Klein, C. Enkrich, M. Wegener, and S. Linden, "Second-harmonic generation from magnetic metamaterials," Science **313**(5786), 502–504 (2006).
18. M. W. Klein, M. Wegener, N. Feth, and S. Linden, "Experiments on second- and third-harmonic generation from magnetic metamaterials," Opt. Express **15**(8), 5238–5247 (2007).

#150743 - $15.00 USD Received 7 Jul 2011; revised 22 Aug 2011; accepted 25 Aug 2011; published 2 Sep 2011

19. M. W. Klein, M. Wegener, N. Feth, and S. Linden, "Experiments on second- and third-harmonic generation from magnetic metamaterials: erratum," Opt. Express **16**(11), 8055 (2008).
20. E. Kim, F. Wang, W. Wu, Z. Yu, and Y. Shen, "Nonlinear optical spectroscopy of photonic metamaterials," Phys. Rev. B **78**(11), 113102 (2008).
21. Simulations were performed using the package CONCERTO 7.0, Vector Field Limited, England, (2008).
22. Handbook of Optical Constants of Solids I, edited by E. D. Palik (Academic, San Diego, 1998).
23. P. B. Johnson and R. W. Christy, "Optical constants of the noble metals," Phys. Rev. B **6**(12), 4370–4379 (1972).
24. J. Rudnick and E. A. Stern, "Second-harmonic radiation from metal surfaces," Phys. Rev. B **4**(12), 4274–4290 (1971).
25. D. Krause, C. W. Teplin, and C. T. Rogers, "Optical surface second harmonic measurements of isotropic thin-film metals: Gold, silver, copper, aluminum, and tantalum," J. Appl. Phys. **96**(7), 3626 (2004).
26. Y. R. Shen, *The Principles of Nonlinear Optics* (Wiley, New York, 1973).
27. This is the simplest way to consider the local field corrections for the SH radiations. Those electric dipoles generated deep inside the structure (say, located at the inner surfaces sandwiched between two silver layers) do not radiate efficiently, and therefore, we do not include their contribution.
28. Because $\chi^{(2)}_{S,\zeta\xi\xi} = \chi^{(2)}_{S,\zeta\eta\eta} = 0$ from the free electron gas model for Ag, the local field component parallel to the surface cannot induce a non-vanishing $p_z^{(2)}$ on the surface. However, a weak local field component perpendicular to the surface is actually present when the S-polarized input impinges on the nanostructure.

1. Introduction

Metamaterials have recently attracted widespread interest due to their intriguing properties not found in ordinary materials. They are artificial electromagnetic (EM) materials composed of subwavelength local resonant structures of electric and/or magnetic type, and can possess arbitrary values of effective permittivity ε and permeability μ dictated by resonant structures. The linear wave properties of metamaterials have been extensively studied in the past several years, with many exciting new phenomena predicted or demonstrated, such as negative refraction [1,2], super lensing [3], optical magnetism [4–12], invisibility cloaking [13,14], subwavelength cavities [15], and so on.

In recent years, there have been a number of reports on studies of nonlinear optical properties of metamaterials. The first attempts were mainly theoretical; experimental works appeared only recently. It was originally suggested by Pendry *et al.* [16] that enhanced nonlinear optical responses could be observed in metamaterials composed of split ring resonators (SRR) at the magnetic resonances. In a series of recent experiments, significantly enhanced second-harmonic generation (SHG) signals were indeed observed in planar arrays of gold SRRs at their magnetic resonance frequencies [17–19], but the SHG signals were obtained at a single frequency. Later, the spectra of SHG around the magnetic resonance for a fishnet metamaterial structure were measured [20], exhibiting strong enhancement at the resonance. It was suggested in Ref [20]. that unlike in a molecular system, the resonant enhancement came from local-field enhancement due to magnetic resonance at the input frequency. However, detailed theoretical calculation in comparison with experiment has not yet been attempted, and quantitative understanding of the observations is still lacking.

In this paper, we report combined theoretical and experimental efforts to study SHG from a fishnet structure with $Ag/SiO_2/Ag$ sandwiched layers. We use a theoretical approach that combines finite-difference-time-domain (FDTD) simulation with a field integration technique to calculate the second harmonic (SH) response from the metamaterial. The calculated SHG spectra around the magnetic resonance show quantitative agreement with the experimentally measured spectra of P and S polarization combinations. The maximum resonance enhancement of SHG reaches ~80 times of that from a flat Ag surface for the P-in/P-out polarization combination, suggesting that metamaterials could be potentially useful as nonlinear optical materials in some applications. Furthermore, the theoretical calculations are able to explain many interesting features observed in experiment, and allow design of structure that maximizes SHG.

The paper is organized as follows. In Sec. II, we describe our calculation methodology and compare the calculated results with experiment on the fishnet metamaterial. Several interesting issues in nonlinear optical properties of metamaterials are then discussed in Sec. III. We summarize our results in the concluding section.

#150743 - $15.00 USD Received 7 Jul 2011; revised 22 Aug 2011; accepted 25 Aug 2011; published 2 Sep 2011

2. Computational methodology and comparisons with experiment

The fishnet structure we studied is sketched in Fig. 1(a). It consists of a sandwiched structure of Ag/SiO_2/Ag layers with an array of periodic square holes. The structure was deposited on a silicon substrate. It was designed to have a magnetic resonance around $1.38\mu m$ when a normally incident beam was linearly polarized along the thin stripes. The approximate geometric shape and dimensions of the structure are described in Fig. 1(a). Such a fishnet structure was fabricated using electron lithography and nano-imprint. The overall size of the sample was $500\times500\ \mu m^2$. Details of the fabrication procedure have been described elsewhere [20]. A scanning electron microscopy (SEM) image of the sample is shown in Fig. 1(b).

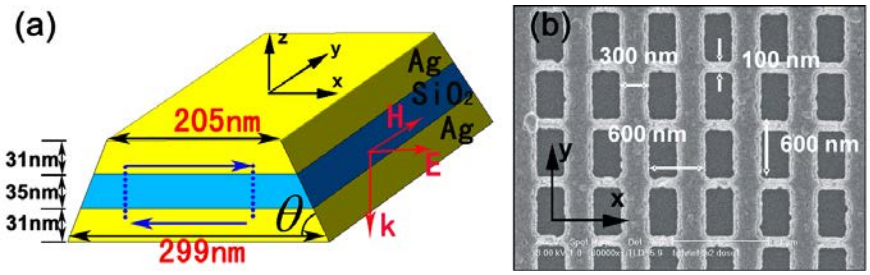

Fig. 1. (a) Cross section of the broad wire of the □shnet structure; (b) SEM image of the □shnet structure.

To understand the nonlinear optical responses of a system, we need to know its linear optical properties first. Therefore, we first discuss comparison of theory with experiment on the linear response of the fishnet sample. We describe here, as a representative case, the response from an input beam with linear polarization along the thin stripes normally impinging on the sample ($\vec{E}\parallel\vec{x}$ and $\vec{H}\parallel\hat{y}$, see Fig. 1(a)). The experiment was carried out with a tunable fiber laser beam focused on the sample. The measured transmission/reflection/absorption spectra are depicted in Fig. 2 by the red open circles, from which a magnetic resonance can be identified at ~1.375μm where the absorbance is maximum. Our theoretical calculation employed the FDTD simulation [21]. In it, the dielectric constants of silicon and silicon dioxide were taken as $3.4777+i0.004$ and 1.65, respectively [22], and we adopted the Drude model to describe the optical dielectric constant of silver $\varepsilon_r(\omega)=\varepsilon_\infty-\omega_{pl}^2/\omega(\omega-i\omega_{col})$ with $\omega_{pl}=1.37\times10^{16}s^{-1}$ and ε_∞ = 4 [23]. For thin silver films used in experiment, we expect electrons to experience additional scattering due to surface roughness and structural imperfections. Therefore, we set the damping parameter ω_{col} as an adjustable parameter to be determined by comparing with the experimental absorption spectrum. We found that the most appropriate value of ω_{col} was $9\times10^{13}s^{-1}$, which is roughly 6.6 times larger than the corresponding bulk value [23]. We note that similar adjustment was adopted in a recent theoretical study [5]. The FDTD calculated spectra with such a choice of ω_{col} are shown in Fig. 2 as blue lines, which are in excellent agreement with the experimental result. FDTD simulations identified the resonance at ~1.375μm to be a fundamental magnetic resonance and that at ~1.02μm a high-order magnetic resonance, since at both wavelengths strongly enhanced magnetic fields are induced inside the sandwich structure while the electric responses in the two Ag layers nearly cancel each other.

#150743 - $15.00 USD Received 7 Jul 2011; revised 22 Aug 2011; accepted 25 Aug 2011; published 2 Sep 2011

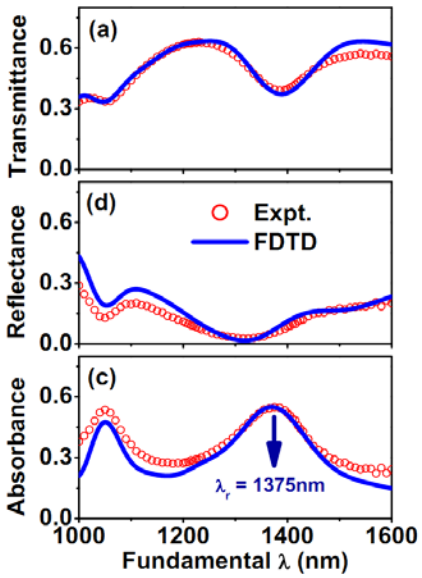

Fig. 2. Linear transmission, reflection and absorption spectra of the double-fishnet metamaterial, obtained by experiments (red circles) and FDTD simulations (blue lines).

We could further employ FDTD simulations to calculate the local electric field distribution of the input in the fishnet structure, which was needed to compute the nonlinear responses of the system. As an example, we show in Fig. 3 the distribution of local electric field on the x-z symmetry plane in the structure, computed at the magnetic resonance frequency under a normally incident radiation with $\vec{E} \| \vec{x}$. We find that the local field is strongly enhanced on the inclined planes in regions close to the boundary between the top Ag layer and the middle SiO_2 layer.

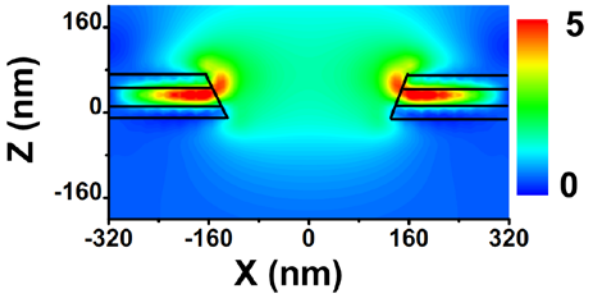

Fig. 3. Normalized electric field distribution on the middle symmetrical x-z plane inside the realistic double-fishnet structure, calculated by FDTD simulations at the magnetic resonance frequency.

Having shown that theoretical calculation on the linear response of the fishnet agrees well with experiment, we now turn to the nonlinear response of the system. We first describe our computational methodology. Stern and Rudnick first formulated the theory of SH response from a metal [24]. They treated the metal as a free electron gas and showed that the nonlinear response arises from variations of electron density and field at the surface along the surface normal and can be described by two independent, non-vanishing surface nonlinear susceptibilities $\chi^{(2)}_{S,\perp} \equiv \chi^{(2)}_{S,\zeta\zeta\zeta}$ and $\chi^{(2)}_{S,\parallel} \equiv \chi^{(2)}_{S,\xi\xi\zeta} = \chi^{(2)}_{S,\xi\zeta\xi} = \chi^{(2)}_{S,\eta\eta\zeta} = \chi^{(2)}_{S,\eta\zeta\eta}$, where ζ is along the surface normal. In a real metal, the inter-band electron transitions may also contribute to the SH response making $\chi^{(2)}_{S,\zeta\xi\xi} = \chi^{(2)}_{S,\zeta\eta\eta}$ non-vanishing, although according to Ref [25], the effect

#150743 - $15.00 USD Received 7 Jul 2011; revised 22 Aug 2011; accepted 25 Aug 2011; published 2 Sep 2011

is expected to be small for Ag. In our calculations, we shall simply assume that $\vec{\vec{\chi}}_S^{(2)}$ of silver is dominated by the free-electron contribution, with susceptibility elements given by Ref [25]. Such an approximation makes the computation much easier to handle.

Assuming $\vec{\vec{\chi}}_S^{(2)}$ discussed above is equally applicable to flat Ag surfaces and local Ag surfaces of the metamaterial structure, we can calculate the effective electric-dipole moment for SH radiation, $\vec{p}^{(2)}(2\omega)$, that is induced in a unit cell by an incoming field, $\vec{E}(\omega)$. Explicitly, we have [20,26]

$$\vec{p}^{(2)} = \int \vec{\vec{L}}(\vec{r}, 2\omega) : \vec{\vec{\chi}}_S^{(2)} : [\vec{E}_{loc}(\vec{r}, \omega)]^2 d\vec{r} \,, \tag{1}$$

where the integration is over the entire silver surfaces within a unit cell, $\vec{E}_{loc}(\vec{r}, \omega) = \vec{\vec{L}}(\vec{r}, \omega) \cdot \vec{E}(\omega)$ is the local electric field, and $\vec{\vec{L}}(\vec{r}, \omega_i)$ is the local field correction factor at ω_i, which can be obtained from calculation of the local-field distribution in the linear response described earlier (see, for example, Fig. 3). Note that resonance of the metamaterial actually appears as resonant enhancement in the local field factor $\vec{\vec{L}}(\vec{r}, \omega)$. Because the metamaterial structure has no resonance at 2ω, $\vec{\vec{L}}(\vec{r}, 2\omega)$ is not as important here as $\vec{\vec{L}}(\vec{r}, \omega)$. For a very rough calculation, we can assume that the integration in Eq. (1) is only over the surface areas of a unit cell that are directly *exposed* to the incoming light [27].

The reflected SH signal from the fishnet, normalized against a reference, which is the reflected SH signal with P-in/P-out polarizations from a flat Ag surface of the same flat area as the fishnet, has the expression

$$\frac{S_{\sigma'\sigma}}{S_{ref}} = \frac{\left|\hat{e}_\sigma \cdot \vec{p}^{(2)}(\sigma, \sigma')\right|^2}{\left|\hat{e}_p \cdot [\vec{p}^{(2)}(p, p)]_{ref}\right|^2} \,. \tag{2}$$

Here, $S_{\sigma'\sigma}$ denotes the signal generated with the σ'-in/σ-out polarization combination, $\hat{e}_\sigma$ (σ = S,P) is the unit vector for polarization σ, and $\vec{p}^{(2)}(\sigma, \sigma')$ and $[\vec{p}^{(2)}(p, p)]_{ref}$ refer to the effective SH dipole moments per unit cell area on the sample and the flat Ag film, respectively, induced by inputs of the same intensity. For $[\vec{p}^{(2)}(p, p)]_{ref}$, Eq. (1) reduces to

$$[\vec{p}^{(2)}(p, p)]_{ref} = A\vec{\vec{L}}(\vec{r}, 2\omega) : \vec{\vec{\chi}}_S^{(2)} : [\vec{\vec{L}}(\vec{r}, \omega) \cdot \vec{E}_p(\omega)]^2, \tag{3}$$

where *A* is the area of the unit cell of the fishnet, and the local-field factor $\vec{\vec{L}}(\vec{r}, \omega)$ is simply the transmission Fresnel coefficient for the air/metal interface.

We calculated the linear response (to deduce the local field distribution) and the reflected SHG spectra with various input/output polarization combinations around the magnetic resonance of the fishnet. The incident plane was chosen to coincide with either the y-z or the x-z plane (x and y being along and perpendicular to the thin stripes, respectively), with the input incident on the sample at an angle of $\alpha = 45^\circ$. The calculated SHG spectra are compared with the experimentally measured spectra in Fig. 4. The (SHG) experiment was carried out using tunable picosecond pulses generated from a Nd:YAG laser-pumped optical parametric system. Detailed experimental arrangement was essentially the same as that described in Ref [20]. Both experiments and computations were carried out at 45 degrees incidence since SHG, by symmetry, is not allowed at normal incidence on an ideal fishnet structure. Inset to Fig. 4 shows the measured quadratic dependence of the SHG signal on the pump power, which is a characteristic feature of SHG. The observed SHG spectra of different polarization combinations, normalized against the SH signal of P-in/P-out polarization combination from a flat Ag film, are presented in Fig. 4. We find reasonable quantitative

#150743 - $15.00 USD Received 7 Jul 2011; revised 22 Aug 2011; accepted 25 Aug 2011; published 2 Sep 2011

agreement between calculated and measured spectra. The non-zero SHG signals in SS and PS cases observed experimentally are caused by imperfections of the real sample.

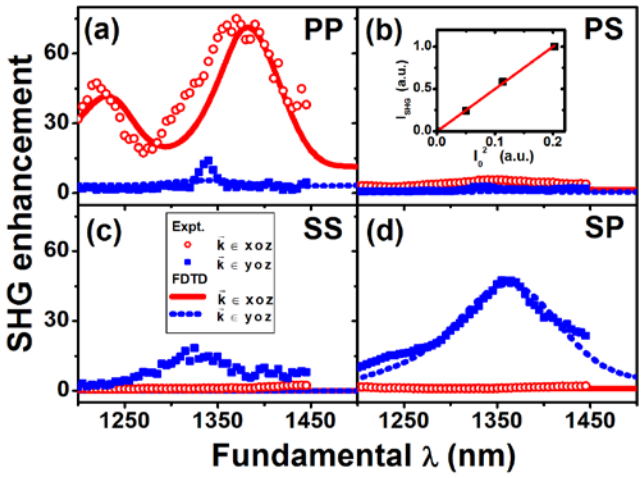

Fig. 4. FDTD calculated (lines) and measured (symbols) SHG spectra of the fishnet structure for different polarization combinations: (a) P in, P out; (b) P in, S out; (c) S in, S out; (d) S in, P out. The incident angle is kept at $\alpha = 45^{\circ}$ and the incident planes are specified in the legend for different cases. Inset shows the measured quadratic dependence of the SHG signal on the incident pump power.

Several characteristic features of the SHG spectra from the fishnet are noticed. First, a resonant peak always appears around the magnetic resonance at $\sim 1.375\mu m$ as long as the input beam has a magnetic field component along $\hat{y}$, although the precise position of the resonance peak shifts slightly in different spectra compared to the normal incidence case (Fig. 2). Second, both theory and experiment show that the SHG enhancement for the P-in/P-out polarizations at the magnetic resonance is ~80 times in comparison with that on a flat silver surface. This is remarkable considering that the fishnet structure has nearly half of the surface plane empty. Third, the P-polarized SH output is much stronger than the S-polarized one, irrespective of the input polarization. Fourth, both theory and experiment display two resonant peeks in the P-in/P-out spectra; the peak at $\sim 1.22\mu m$ was *not* observed in the normal incidence spectra (Fig. 2) and the S-in/P-out SHG spectrum (Fig. 4(d)). Finally, the non-resonant SH signal with P-in/P-out polarizations is strong as we would expect, knowing that a strong PP-SHG is also observed on a flat silver film. We shall discuss our understanding of these features in the following section.

3. Discussions

The resonant enhancement of SHG from the fishnet around the magnetic resonance at $\sim 1.375\mu m$ arises from resonant enhancement of the local field. For our fishnet structure, the magnetic resonance can be excited only when the input excitation has a magnetic field component along $\hat{y}$, and is observable in SHG with a P-polarized input propagating in the x-z plane or an S-polarized input propagating in the y-z plane. To explicitly illustrate the local field enhancement effect, we depict in Fig. 5(a) and (b) the FDTD-calculated local field (normalized by the incoming field) at the upper Ag/SiO_2 edge on the inclined side plane versus fundamental wavelength λ for S-polarized input in the y-z plane and P-polarized input in the x-z plane, respectively. In both cases, the fundamental resonance at $\sim 1.375\mu m$ is obvious. Interestingly, an additional weak resonance at $\sim 1.22\mu m$ is found in the P-input case

#150743 - $15.00 USD Received 7 Jul 2011; revised 22 Aug 2011; accepted 25 Aug 2011; published 2 Sep 2011

(Fig. 5(b)), which does not exist in the S-input spectra (Fig. 5(a)) and the normal-incidence spectrum (Fig. 2(c)). FDTD simulations identified this resonance as an electric-dipole one with currents flowing on the side walls, and it can only be excited by an input wave with an E_z component (e.g., off-normal P-wave input). This resonance is also responsible for the peak at $\sim 1.22\mu m$ in the PP-SHG spectra (Fig. 4(a)), observed both experimentally and numerically. We note that the frequencies of resonances excited by S- and P-polarized inputs are slightly different (Fig. 5), and similarly for resonances observed in the SHG spectra with S- and P- inputs as shown in Fig. 4(a) and (d). This is due to different resonance dispersions in the two cases because of different couplings between adjacent magnetic resonators in the fishnet. Both experiment and FDTD simulation revealed that the resonance dispersion of the S-input case is stronger than that of the P-input case, and consequently, at an incident angle 45°, the former has a resonance frequency more red-shifted than the latter. The FDTD simulations have taken such effects into account rigorously. To be sure that the resonant peak at $1.375\mu m$ is from the magnetic resonance of the double-layer fishnet, we calculated SHG from a single fishnet layer which cannot support a magnetic resonance. As expected, no such peak can be detected.

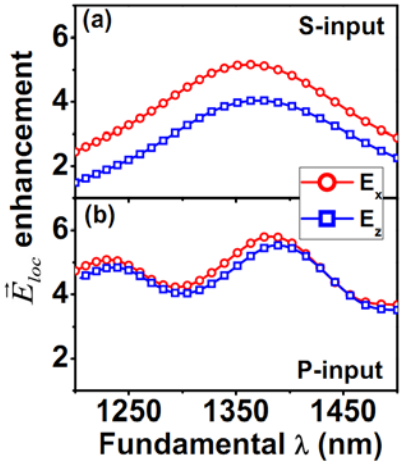

Fig. 5. Normalized local fields at the Ag/SiO_2 edge in the inclined side plane as functions of the fundamental wavelength, calculated by FDTD simulations assuming (a) S-wave incident in the y-z plane and (b) P-wave incident in the x-z plane.

In principle, the local-field factor $\ddot{L}(\vec{r},\omega)$ can be derived from the fields as depicted in Fig. 5(a) and (b), and $\ddot{L}(\vec{r},\omega)$ can be approximated by

$$\ddot{L}(\vec{r},\omega) \approx \ddot{A}(\vec{r}) + \frac{\ddot{B}(\vec{r})}{\omega - \omega_r + i\Gamma}, \tag{4}$$

at frequencies around the fundamental resonant frequency ω_r. Since $\vec{p}^{(2)}(2\omega)$ in Eq. (1) has its integrand proportional to $[\ddot{L}(\vec{r},\omega)]^2$, we should expect a significantly stronger resonant enhancement in SHG than in $\ddot{L}(\vec{r},\omega)$. Comparisons of Figs. 5 and 4 show that this is indeed the case.

The relative strengths of SHG with different polarization combinations can be understood from symmetry argument. We notice that Eq. (1) can be re-written as

$$\vec{p}^{(2)}(2\omega) = \ddot{\chi}^{(2)} : \vec{E}(\omega)\vec{E}(\omega), \tag{5}$$

#150743 - $15.00 USD Received 7 Jul 2011; revised 22 Aug 2011; accepted 25 Aug 2011; published 2 Sep 2011

where $\vec{\vec{X}}^{(2)} = \int \vec{L}(\vec{r},2\omega) : \vec{\vec{\chi}}_S^{(2)} : \left[\vec{L}(\vec{r},\omega)\right]^2 d\vec{r}$ should reflect the symmetry of the unit cell. If the fishnet structure of Fig. 1 has mirror planes at x = 0 and y = 0, then the nonvanishing elements of $\vec{\vec{X}}^{(2)}$ are $X_{zzz}^{(2)}$, $X_{zxx}^{(2)}$, $X_{zyy}^{(2)}$, $X_{xzx}^{(2)} = X_{xxz}^{(2)}$, and $X_{yzy}^{(2)} = X_{yyz}^{(2)}$. None of these elements contributes to SHG with P(-in)S(-out) and SS polarization combinations. Therefore, PS-SHG and SS-SHG are forbidden in such a fishnet structure. The experimentally observed signals shown in Fig. 4 appeared only because our real fishnet structure did not have the perfect mirror symmetry. On the other hand, SP- and PP-SHG are allowed. As mentioned above, the magnetic resonance is expected in SP-SHG with beams in the y-z plane and in PP-SHG with beams in the x-z plane. The corresponding contributing $\vec{\vec{X}}^{(2)}$ elements to SP-SHG and PP-SHG are $X_{zxx}^{(2)}$ and ($X_{zzz}^{(2)}$, $X_{zxx}^{(2)}$, $X_{xzx}^{(2)} = X_{xxz}^{(2)}$), respectively. We note here that in contrast to the flat metal surface, SP-SHG from the fishnet (with beams in the y-z plane) is non-vanishing even if we treat the metal as a free electron gas (see Sec. 2). This is mainly because SP-SHG can be generated from the inclined side planes of the fishnet structure. In our fishnet structure, SHG originates from the silver part of the surfaces. For SP-SHG, the P-polarized SH output comes solely from $p_z^{(2)}$ induced in each unit cell by the S-polarized input. Contribution from the top flat surface of the Ag stripes to $p_z^{(2)}$ is negligible if the local field component perpendicular to the surface is negligible [28]. On the other hand, contribution from the Ag side planes is significant and is given by

$$p_z^{(2)} \sim \int \left\{ \begin{array}{l} \chi_{\perp}^{(2)} (E_{z,loc}\cos\theta + E_{x,loc}\sin\theta)^2 \cos\theta \\ -2\chi_{\parallel}^{(2)} (E_{x,loc}\cos\theta - E_{z,loc}\sin\theta)(E_{z,loc}\cos\theta + E_{x,loc}\sin\theta)\sin\theta \end{array} \right\} dS, \quad (6)$$

where θ is the inclination angle of the side planes (see Fig. 1), and the integration is over the Ag-covered area of the inclined side planes. Figure 6 shows how $E_{x,loc}$ and $E_{z,loc}$ vary on the side wall and the top Ag surface for $\theta = 71^\circ$ (experimental sample) and $\theta = 90^\circ$ (ideal case with vertical side wall). It is seen that around the upper Ag/ SiO_2 edge on the side walls, the local field enhancement is near maximum. In addition, different symmetry properties possessed by $E_{x,loc}$ and $E_{z,loc}$ within a unit cell are actually responsible for the global symmetry of $\vec{\vec{X}}^{(2)}$ elements which we argued before. At $\theta = 90^\circ$, both $E_{x,loc}$ and $E_{z,loc}$ are present even though the S-polarized input has *only* a field component along $\hat{x}$.

#150743 - $15.00 USD Received 7 Jul 2011; revised 22 Aug 2011; accepted 25 Aug 2011; published 2 Sep 2011

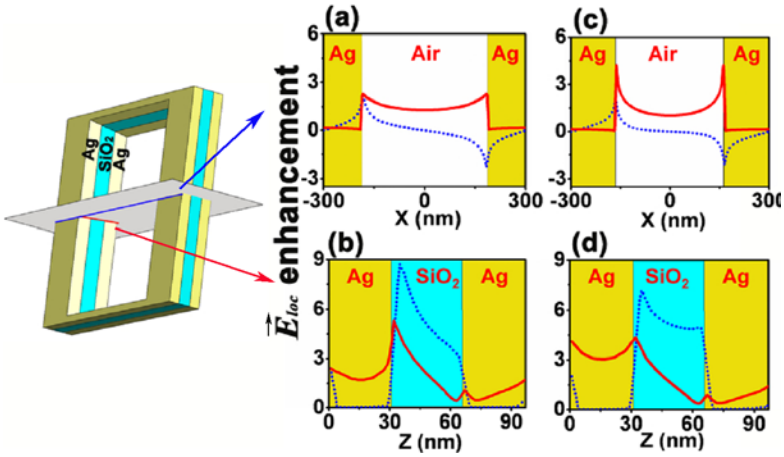

Fig. 6. Distributions of normalized local fields (solid line: $E_{x,loc}$; dashed line: $E_{z,loc}$) along the symmetry lines on the top and the side wall Ag surface (see left panel), calculated by FDTD simulations for the fishnet structures with (a) + (b) $\theta = 71^{\circ}$, and (c) + (d) $\theta = 90^{\circ}$.

Figure 7 describes SHG from a fishnet with $\theta = 90^{\circ}$ obtained from FDTD simulations. It is seen, as expected, that SS- and PS-SHG do vanish, consistent with the symmetry argument presented above. Both PP- and PS-SHG are allowed, but PP-SHG is appreciably stronger than SP-SHG. It is interesting to compare the $\theta = 90^{\circ}$ case (Fig. 7) with the experimental sample case with $\theta = 71^{\circ}$ (Fig. 4). Because of the much stronger local-field enhancement, PP-SHG and SP-SHG for $\theta = 71^{\circ}$ are much stronger than those for $\theta = 90^{\circ}$.

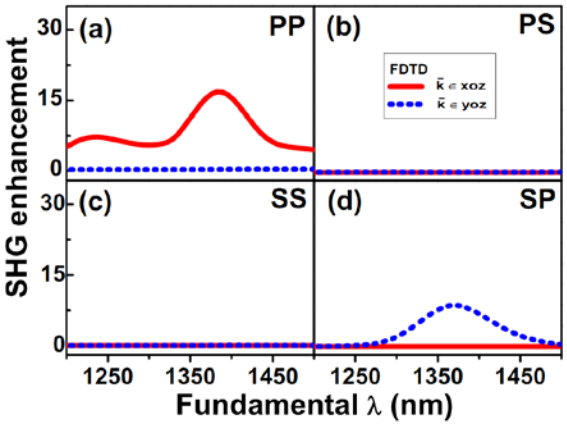

Fig. 7. FDTD simulated SHG spectra of the perfect fishnet structure (with vertical side walls) for different polarization combinations: (a) P in P out, (b) P in S out, (c) S in S out, and (d) S in P out. Here, the incident angle is kept as $\alpha = 45^{\circ}$ and the incident planes are specified in the legend for symbols and lines, respectively.

To illustrate how the local field on the side wall depends on the inclination angle θ, we studied a series of fishnets with different θ (by varying the width of the top metal stripes and keeping that of the bottom metal stripes fixed). Figure 8(a) depicts how $E_{x,loc}$ and $E_{z,loc}$ at the upper Ag/ SiO_2 edge on the side wall vary with θ; they first increase with θ, and then decrease after reaching a maximum at $\theta \sim 72^{\circ}$. The appearance of an optimistic angle exhibiting the strongest field enhancement is the result of competition between two factors:

#150743 - $15.00 USD Received 7 Jul 2011; revised 22 Aug 2011; accepted 25 Aug 2011; published 2 Sep 2011

As θ increases, the top silver area shrinks (to zero at $\theta \sim 33^{\circ}$, see Fig. 1(a)), and accordingly, the strength of the magnetic resonance decreases. On the other hand, the geometric coupling between external radiation and the magnetic resonance increases with θ. Since SHG in a fishnet is mainly governed by the resonantly enhanced local field, we expect a similar dependence of SHG on θ. Figure 8(b) shows how PP-SHG at resonance varies with θ, and indeed its maximum also appears at $\theta \sim 72^{\circ}$. We note here that as seen from Fig. 6, the local-filed distribution on the fishnet structure is very strong in the region of the sandwiched dielectric medium on the side walls. Therefore, we should expect also a significant enhancement of SHG from the fishnet if the dielectric medium is highly nonlinearly active.

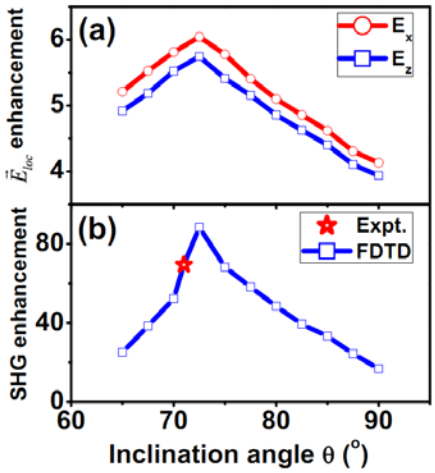

Fig. 8. (a) Normalized local-field resonance enhancements at the upper Ag/SiO_2 edge on the side wall as functions of inclination angle θ of the fishnet structure, calculated by FDTD simulations assuming a P-wave input. (b) FDTD calculated peak PP-SHG value as a function of θ, with the red star indicating the experimental situation.

We can use a crude approximation to derive a simple equation to describe the SHG spectra. We notice in Figs. 3 and 6 that the local field exhibits "hot-spots" near the upper Ag/SiO_2 edge on the side walls. Assuming SHG mainly comes from such "hot-spots" in the fishnet, we then expect the SH output, S, to be proportional to $|\vec{E}_{loc}(\omega)|^4$ or $|L(\omega)|^4$ at the "hot-spots". We can then write, following Eq. (4) and considering the presence of two resonances (at ~ and ~1.22μm) in the P-input case (see Figs. 4 and 5(a)),

$$S^{PP}(\omega) = [B + \frac{C}{\omega - \omega_1 + i\Gamma} + \frac{D}{\omega - \omega_2 + i\Gamma}]^4, \qquad (7)$$

where B describes the non-resonant contribution and C and D are the strengths of the two resonances. The spectrum calculated with Eq. (7), using $B = 0.775$, $C = 29\text{THz}$, $D = 14\text{THz}$, $\omega_1 = 218\text{THz}$, $\omega_2 = 245\text{THz}$, and $\Gamma = 10.8\text{THz}$, is plotted in Fig. 9 as a black solid line, which appears to be in good agreement with both experiment and FDTD simulation.

#150743 - $15.00 USD Received 7 Jul 2011; revised 22 Aug 2011; accepted 25 Aug 2011; published 2 Sep 2011

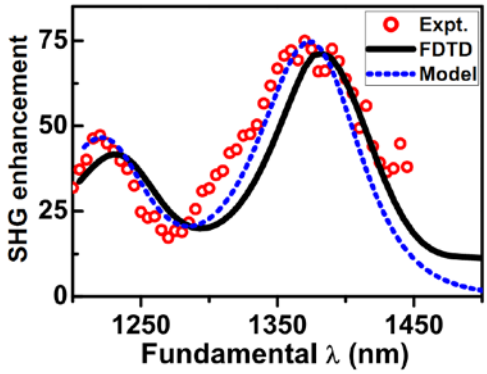

Fig. 9. PP-SHG spectra of the fishnet structure, obtained by FDTD simulations, experimental measurements and the analytical model.

We note that the bandwidth of the measured SHG peak (Fig. 4) is narrower than the linear absorption peak (Fig. 2). It was shown in Ref [20]. that the measured third harmonic generation (THG) peak is further narrowed compared with the SHG one. This is in striking contrast with resonance behaviors of molecular materials, where the linear, SHG, and THG spectra often have similar line shapes [26]. The difference arises because in metamaterials, the resonance enhancement is through the local field resonance. The *n*th harmonic in a metamaterial is generated by the *n*th-order induced polarization $\vec{p}^{(n)} = \int \vec{\vec{L}}(\vec{r}, n\omega) : \vec{\vec{\chi}}^{(n)}_{eff}(\vec{r}) : [\vec{E}_{loc}(\vec{r}, \omega)]^n d\vec{r}$, which can be approximated by $p^{(n)}(n\omega) \propto \left|\vec{\vec{L}}(\vec{r}, \omega)\right|^n$ if "hot spots" exist. This explains the resonant linewidth narrowing of the higher harmonics.

For the sample studied in this paper, our calculation does not show the existence of an SH resonance in the frequency range we probed. The observed resonant spectral profile and its agreement with theory also indicate that the SH resonance did not occur in our sample. However, we could adjust the hole size of the fishnet to have resonances at both ω_r and $2\omega_r$. In that case, we need to also include the resonantly enhanced local field correction term $\vec{\vec{L}}(\vec{r}, 2\omega)$ in the calculation.

4. Conclusions

In summary, we have presented in this paper a complete analysis of second harmonic responses from fishnet metamaterials. By combining FDTD simulations with a field integration technique, we establish a computational approach to calculate the SHG spectra from the metamaterials, and find that the results are in reasonable agreement with experimental data. The resonant enhancement of SHG from a metamaterial is through the resonant enhancement of the local field, and is dominated by the strongly enhanced local field at "hot spots". The theoretical calculations also help us understand the details of many interesting phenomena observed experimentally, and allow us to design optimal structures that would yield the highest harmonic or other wave mixing outputs.

Acknowledgments

This work was supported by the National Science Foundation of China (60725417, 60990321, 11174055), MOE of China (B06011), and Shanghai Science and Technology Committee (08dj1400302). DC and YRS acknowledge support from the Director, Office of Science, Office of Basic Energy Sciences, Materials Sciences and Engineering Division, of the U.S. Department of Energy under Contract No. DE-AC03-76SF00098.

#150743 - $15.00 USD Received 7 Jul 2011; revised 22 Aug 2011; accepted 25 Aug 2011; published 2 Sep 2011